Supporting Information

Pyrene based fluorescent Ru(II)-arene complexes towards significant biological applications: catalytic potential, DNA/protein binding, two photon cell imaging and *in vitro* cytotoxicity

Pragti,[a] Bidyut Kumar Kundu,[ab] Shrish Nath Upadhyay,[c] Nilima Sinha,[c] Rakesh Ganguly,[d] Ivo Grabchev,[e] Srimanta Pakhira,[cfg] * Suman Mukhopadhyay[a]*

* = Corresponding authors

[a] Department of Chemistry, School of Basic Sciences, Indian Institute of Technology Indore, Simrol, Khandwa Road, Indore 453552, India.

[b] Department of Chemistry, University of Cincinnati, Cincinnati, OH, 45221, USA.

[c] Department of Metallurgy Engineering and Materials Science (MEMS), Indian Institute of Technology Indore, Indore-453552, MP, India.

[d] Shiv Nadar University, Greater Noida, 201314, India.

[e] Sofia University "St. Kliment Ohridski" Faculty of Medicine, 1, Koziak Str., 1407 Sofia, Bulgaria.

[f] Department of Physics, Indian Institute of Technology Indore (IITI), Simrol, Khandwa Road, Indore-453552, MP, India.

[g] Centre for Advanced Electronics (CAE), Indian Institute of Technology Indore, Indore-453552, MP, India.

*E-mail: : : spakhira@iiti.ac.in or spakhirafsu@gmail.com (S.P.) and suman@iiti.ac.in (S.M.); Fax: +91 731 2361; Tel: +91 731 2438 735

Table of Contents

Section S1. Abbreviation used in this article

Entry	Significance	Entry	Significance
HL	(*E*)-N'-(pyren-1-ylmethylene) thiopene-2-carbohyrazide	**HSA**	Human serum albumin
NMR	Nuclear magnetic resonance	**DAPI**	4′,6-diamidino-2-phenylindole
ESI-MS	Electrospray ionisation mass spectrometry	**PI**	Propium iodide
FTIR	Fourier transformed infra-red	**r.t.**	Room temperature

XRD	X-ray diffraction	**FL**	Fluorescence
CT-DNA	calf thymus deoxyribonucleic acid	**MTT**	3-(4,5-dimethylthiazol-2-yl)-2,5-diphenyl tetrazolium bromide
BSA	Bovine serum albumin	**EtBr**	Ethidium Bromide
AO	Acridine Orange		

Section S2. Experimental section

Instrumentation

All the chemicals required are purchased from Sigma and used without further purification. Chemical for biological experiments (3-(4,5-dimethylthiazol-2-yl)-2,5-diphenyltetrazolium bromide (MTT), PBS buffer were purchased from Himedia chemical, India. An AVANCE III 400 Ascend Bruker BioSpin spectrometer was used to record ^{1}H and ^{13}C NMR spectroscopy at room temperature. Infrared (FTIR) spectra (range: 4000 to 500 cm^{-1}) was conducted on BRUKER TENSOR 27 instrument. Elemental analyses (C, H, N and S content) were performed with a MicroTOF-Q II mass spectrometer and ThermoFlash 2000 elemental analyzer. ESI-MS were carried out on Bruker-Daltonics. Spectrophotometric measurements for absorption study were done by using a quartz cuvette with a path length of 1 cm on a Varian UV-Vis spectrophotometer (Model: Cary 100). A Perkin-Elmer lambda-650 DRS UV-Vis spectrophotometer, equipped with an integration sphere diffuse reflectance attachment in the range of 200-1200 nm against $BaSO_4$ as reference was utilized for UV-Vis diffuse reflectance spectral (UV-Vis/ DRS) analyses. The far-ultraviolet (UV) (190 to 260 nm) spectra were recorded in 0.1 cm path length cell (Hellma, Muellheim/Baden, Germany) using a step size of 0.5 nm, bandwidth of 1 nm and a scan rate of 20 nm min^{-1}. Fluorescence emission spectra were recorded at 25.0 ± 0.2 ºC on a Fluoromax-4p spectrofluorometer from Horiba JobinYvon (Model: FM-100) using a quartz cuvette with a path length of 2 cm. Staining assay were done with the help of confocal microscope Fluoview FV100 (OLYMPUS, 449 Tokyo, Japan).

X-ray crystallography

The crystals were mounted onto quartz fibers and the X-ray diffraction intensity data were measured at 293 K with a Bruker APEX II diffractometer equipped with a CCD detector, employing Mo Kα radiation (λ = 0.71073 Å), with the SMART suite of programs.[1] All data were processed and corrected for Lorentz and polarization effects with SAINT and for absorption effects with SADABS.[2] Structure solution and refinement were carried out with

the SHELXTL suite of programs.[3] Data were corrected for absorption effects using the multi-scan method (SADABS). The structures were solved by Patterson maps to locate the heavy atoms, followed by difference maps for the light, non-hydrogen atoms. All non-hydrogen atoms were refined with anisotropic thermal parameters.

Section S3. Experimental Methods

S3.1 Protein Binding Study

S3.1.1 Competitive binding experiments

Protein binding studies of the synthesized compounds were carried out by tryptophan fluorescence quenching experiments using human serum albumin (HSA). The excitation wavelength for HSA was at 280 nm, and the quenching of the emission intensity of the tryptophan residues of HSA at 345 nm was monitored using the complexes as a quencher with increased concentration. The excitation and emission slit widths and scan rates were kept constant throughout the experiment. A 10 μM stock solution of HSA was prepared using 50 mM Tris buffer solution and stored at 4 °C for further use. Stock solutions of 5 mM strength were made using synthesized compounds. Fluorometric titration was carried out taking 2 mL of the protein solution and the fluorescence intensity was measured as blank. For titration, each time, 5 μL of the stock solution was added to the protein solution and the fluorescence intensity was measured. For all the four complexes, up to 50 μL of the solution was added to measure fluorescence quenching. The fluorescence quenching data were further analyzed by using the Stern–Volmer equation, which again can be expressed in terms of the bimolecular quenching rate constant and the average life time of the fluorophore as shown in the following equation:

$F_0/F = 1 + K_{sv}[Q] = 1 + K_q \tau_0 [Q]$…… (1)[4]

where F0 and F are the fluorescence intensities in the absence and presence of a quencher, Kq is the bimolecular quenching rate constant, τ0 is the average lifetime of a fluorophore in the absence of a quencher and [Q] is the concentration of a quencher (metal complexes). K_{SV} is the Stern–Volmer quenching constant in M^{-1}. The binding constant K_a and number of complex bound to BSA (n) are calculated using the following formula.

$log [(F0 - F)/F] = log K_a + n log [Q]$….. (2)[5]

The magnitudes of K_a and K_q of complexes are 10^5 M^{-1} and 10^{13} $M^{-1}s^{-1}$, respectively, indicating a good binding ability to serum protein.

S3.1.2 Circular dichroic spectral studies

Monitoring the far UV-CD spectra (190-250 nm) provides important information to get insight about the change in secondary structure of serum albumin proteins. At first the spectra

of free BSA (10μM) and HSA (10μM) was recorded and then changes in CD spectra were obtained by monitoring the binding of metal complexes upon addition of 20 μM of metal complexes successively. For titration, each time, 5 μL of the stock solution was added to the protein solution and the ellipticity (θ) in CD spectra was measured.[5]

S3.2 DNA binding study

S3.2.1 Absorption spectral studies

The interaction between metal complexes and DNA were studied using electronic absorption method. Disodium salt of calf thymus CT-DNA was stored at 4 ºC. Solution of CT-DNA in the buffer 50 mM NaCl/ 5 mM Tris (pH 7.2) in water gave a ratio 1.9 of UV absorbance at 260 and 280 nm (A260/A280, A = absorbance), indicating that the DNA was sufficiently free from protein[34]. The concentration of DNA was measured using its extinction coefficient (ϵ) at 260 nm after 1:100 dilutions[35]. Stock solutions were stored at 4˚C and used for not more than 4 days. Concentrated stock solutions of the complexes were prepared by dissolving the complexes in DMSO and diluting suitably with the corresponding buffer to the required concentration for all of the measurements. Absorption spectra titrations were performed at room temperature in Tris HCl/ NaCl buffer (5 mM/ 50 mM buffer, pH 7.4) to investigate the binding affinity between CT-DNA and complex. A fixed concentration of the complex (10 μM) was titrated with increasing amounts of CT-DNA concentration. The intrinsic binding constant for the interaction of complex with CT-DNA was obtained from absorption spectral data.[4]

S3.2.2 Competitive binding experiments

The relative binding of complex to CT-DNA were determined with an EB-bound CT-DNA solution in Tris-HCl/ NaCl buffer (5 mM/ 50 mM, pH=7.4). DNA was pre-treated with ethidium bromide for 30 min by maintaining the fixed ratio of [DNA]/ [EtBr] = 2.0. The fluorescence quenching effect on addition of complex to the EB-DNA complex have been analysed by recording the fluorescence emission spectra with excitation at 510 nm and emission at 596 - 600 nm. The titration quenching experiment was carried out by keeping the concentration of DNA in buffer constant and adding 10 μL of the sample solution at a time. After addition of the sample solution, the solution was kept for 1 min and then fluorescence intensity was measured. The quenching efficiency was calculated from Stern-Volmer (SV) equation.

S3.3 Methodology and Computational Details:

Periodic DFT Calculations:

To obtain the equilibrium crystal structures and lattice parameters of both the Complex **1** and Complex **2,** the periodic hybrid density functional theory (DFT) method was employed. The equilibrium geometries with the bulk 3D crystal unit cells of these Complex **1** and Complex **2** were obtained by using first-principles based B3LYP-D3 (in short DFT-D) method employed in quantum chemistry *ab-initio* based CRYSTAL17 program i.e. suite code. Triple-ζ valence polarization (TZVP) quality Gaussian types of atomic basis sets (i.e. Gaussian types of atomic Orbitals (GTO)) of the Ru, S, Cl, N, O and C atoms were used in the present calculations. The equilibrium structures are shown in Fig. S13 and S14. To get fine equilibrium geometry of the crystal structures of the complexes **1** and **2**, semi-empirical Grimme's 3rd order (-D3) dispersion corrections have been incorporated in the present DFT computations to take account weak van der Waals (vdW) interactions among various layers and atoms of the crystals which cannot be avoided. A threshold value of 10^{-7} a. u. was set to converge both the energy and density during the optimization. The importance of B3LYP-D3 method is that it provides excellent quality of geometry of the crystal structures and also the structures are less affected due to the spin contaminations in the calculation. For analysis and graphical representation of the optimized crystal structures VESTA visualization code has been used.

Non-periodic DFT Calculations:

To explore the reaction mechanism involved in the formation of Ruthenium arene complexes, a theoretical and computational study was accomplished by employing the first-principle based hybrid quantum mechanical DFT method i.e. B3LYP considering a non-periodic molecular modeling. All the geometries of ligand HL, ruthenium dimers i.e. $[(\eta^6\text{-p-cymene})RuCl_2]_2$, $[(\eta^6\text{-benzene})RuCl_2]_2$, $[(\eta^6\text{-p-cymene})Ru(N_3)_2]_2$, $[(\eta^6\text{-benzene})Ru(N_3)_2]_2$ and ruthenium arene complexes (i.e. finite molecular cluster model systems of the complexes **1-4** i.e. Complex **1**, Complex **2**, Complex **3** and Complex **4**) were obtained by the same DFT method. The important stationary points on potential energy surface that is energy minima and first order saddle points (i.e., equilibrium transition states (TSs)) was investigated by employing the same DFT method in this study. All the electronic structure calculations and thermodynamic properties of the systems were calculated using B3LYP DFT method by with the Gaussian basis sets i.e., LANL2DZ with the Effective Core Potential (ECP) for the Ru atoms and the 6-31+G* basis sets for the other atoms i.e., C, H, N, O, Cl and S atoms. The harmonic vibrational frequency analysis has been carried out to obtain the energy minima of the equilibrium geometries, and the imaginary frequencies were eliminated very carefully in the optimized stable structures. B3LYP method is the most

popular method because of its accuracy and the equilibrium structures calculated by the B3LYP method are less influenced by the spin contamination in the present DFT calculations.

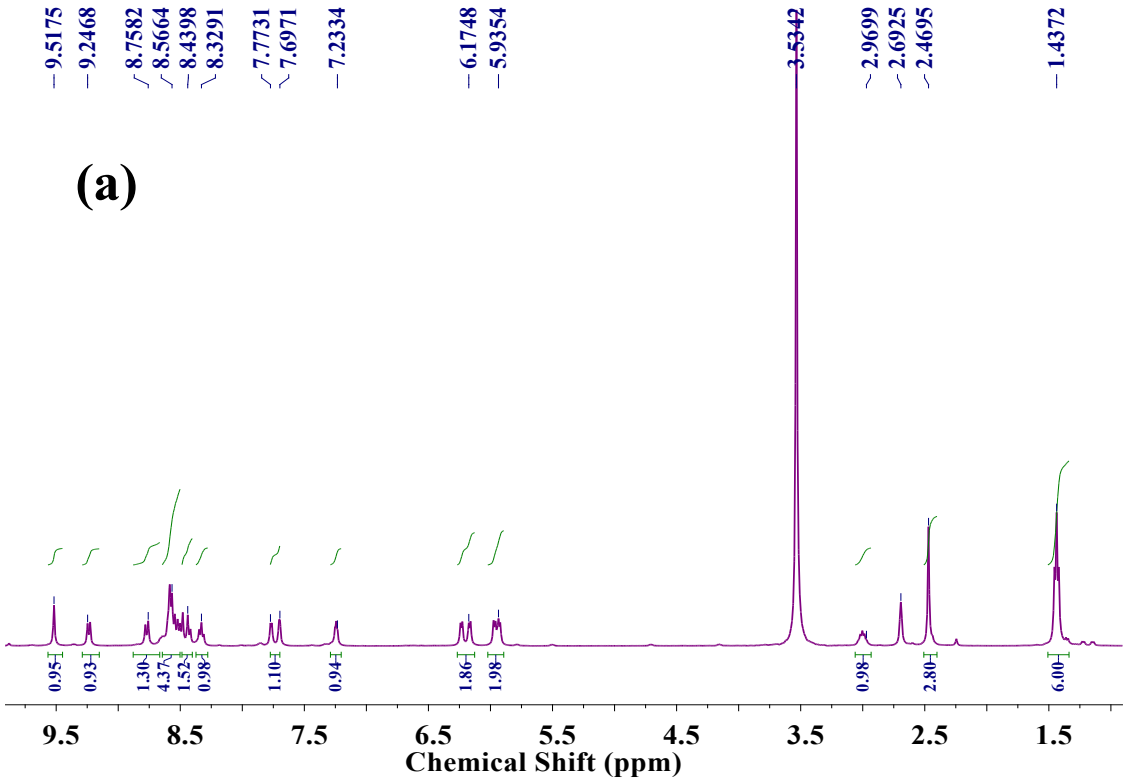

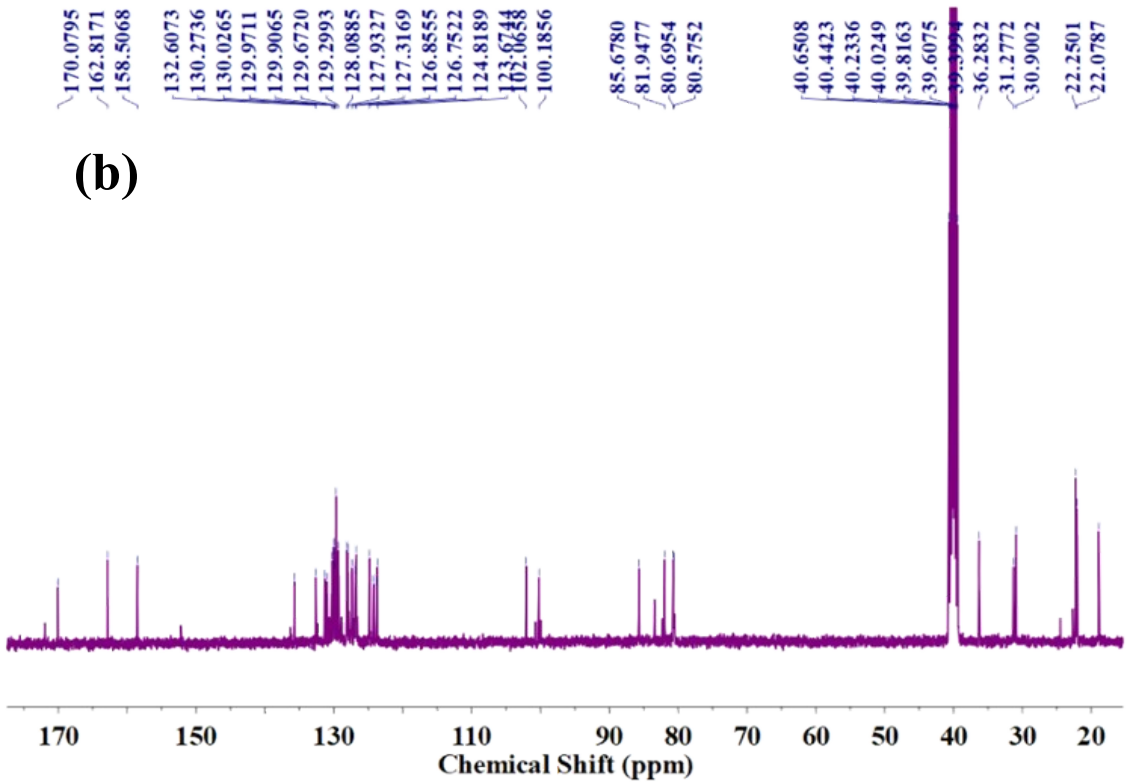

Fig. S1 NMR Spectra of Complex **1** in DMSO-d_6 (400.13 MHz, 298K): (a) ^{1}H NMR and (b) ^{13}C NMR.

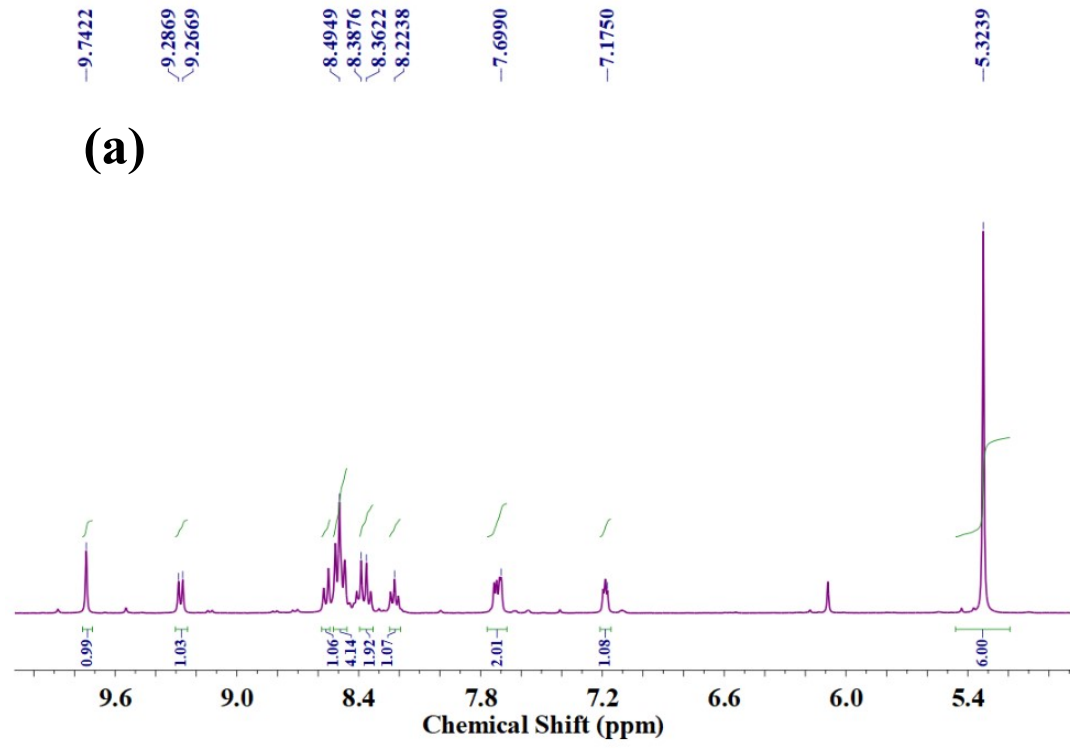

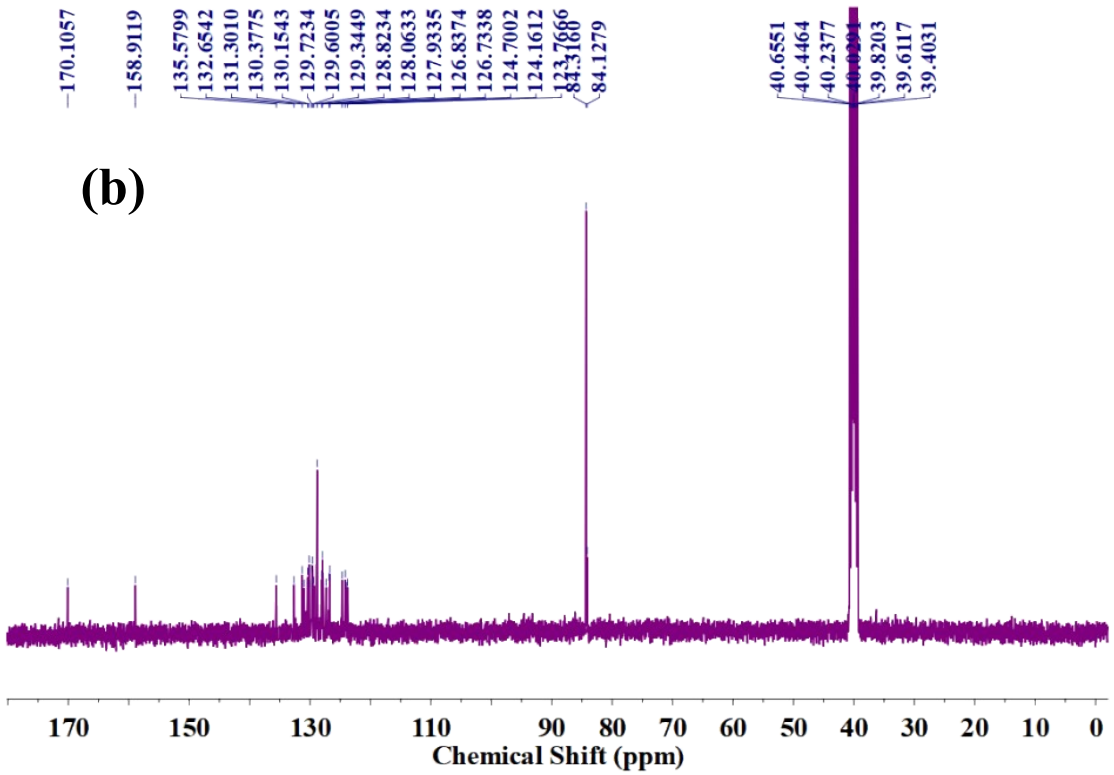

Fig. S2 NMR Spectra of Complex **2** in DMSO-d_6 (400.13 MHz, 298K): (a) ^{1}H NMR and (b) ^{13}C NMR.

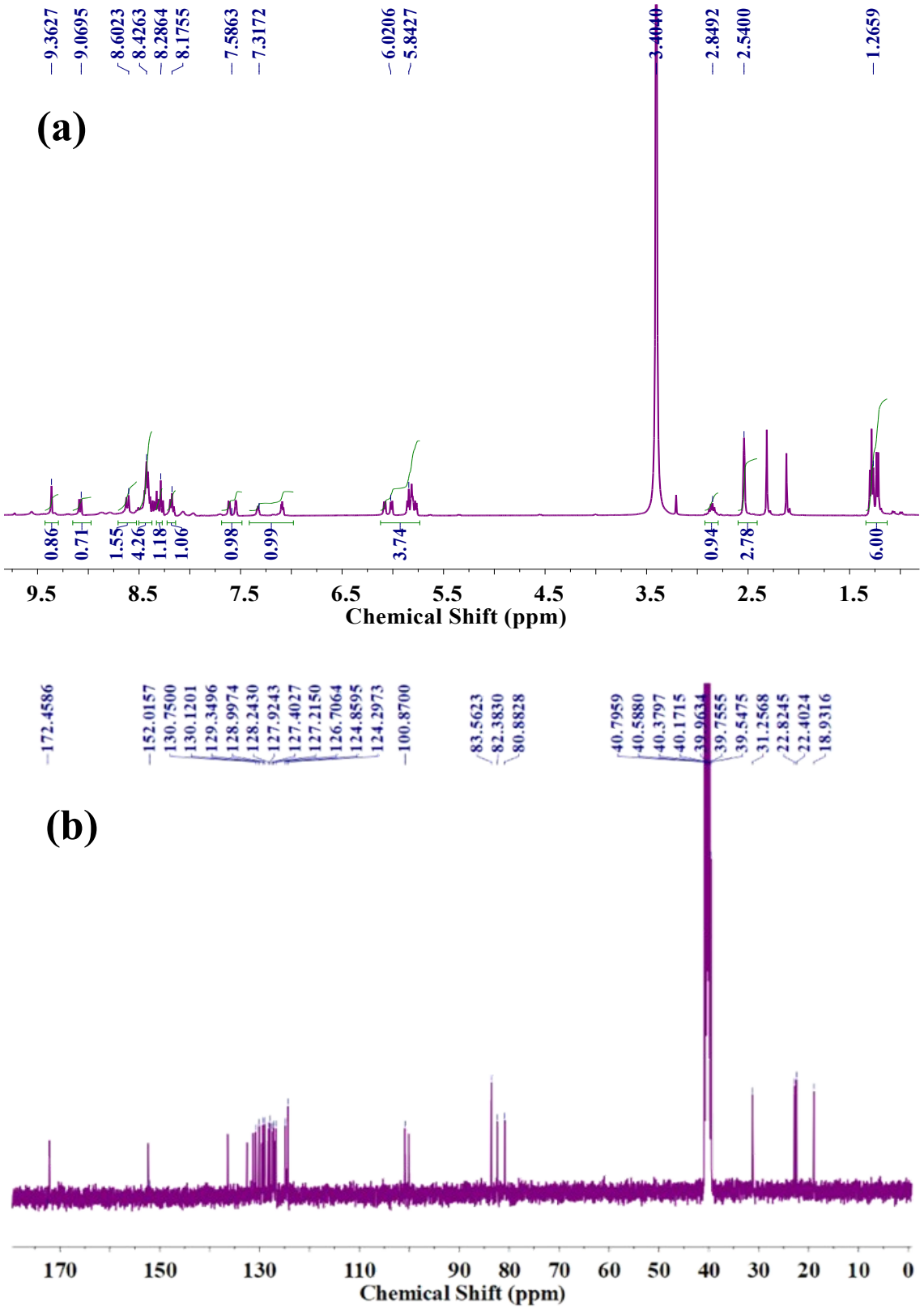

Fig. S3 NMR Spectra of Complex **3** in DMSO-d_6 (400.13 MHz, 298K): (a) ^{1}H NMR and (b) ^{13}C NMR.

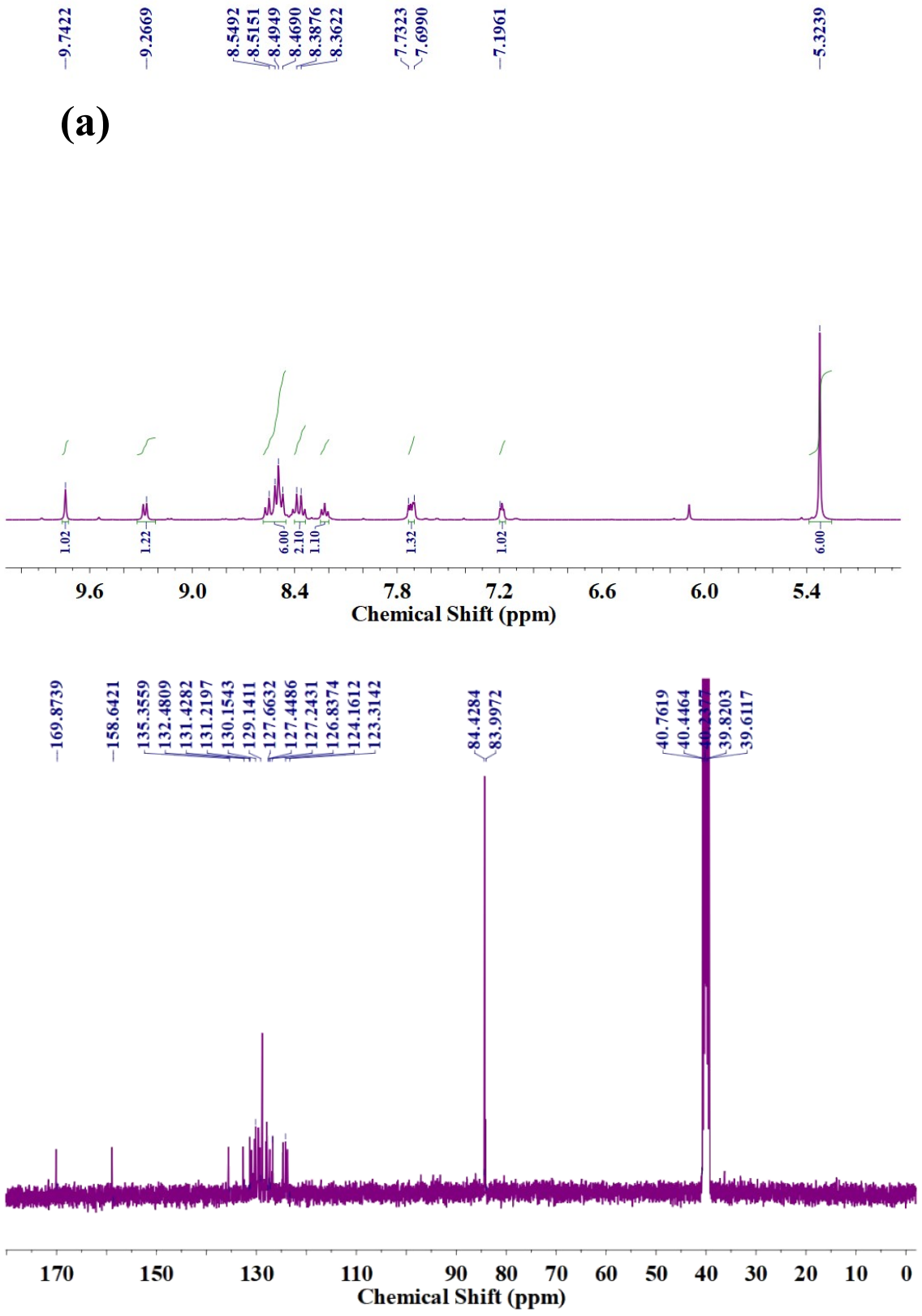

Fig. S4 NMR Spectra of Complex **4** in DMSO-d_6 (400.13 MHz, 298K): (a) ^{1}H NMR and (b) ^{13}C NMR.

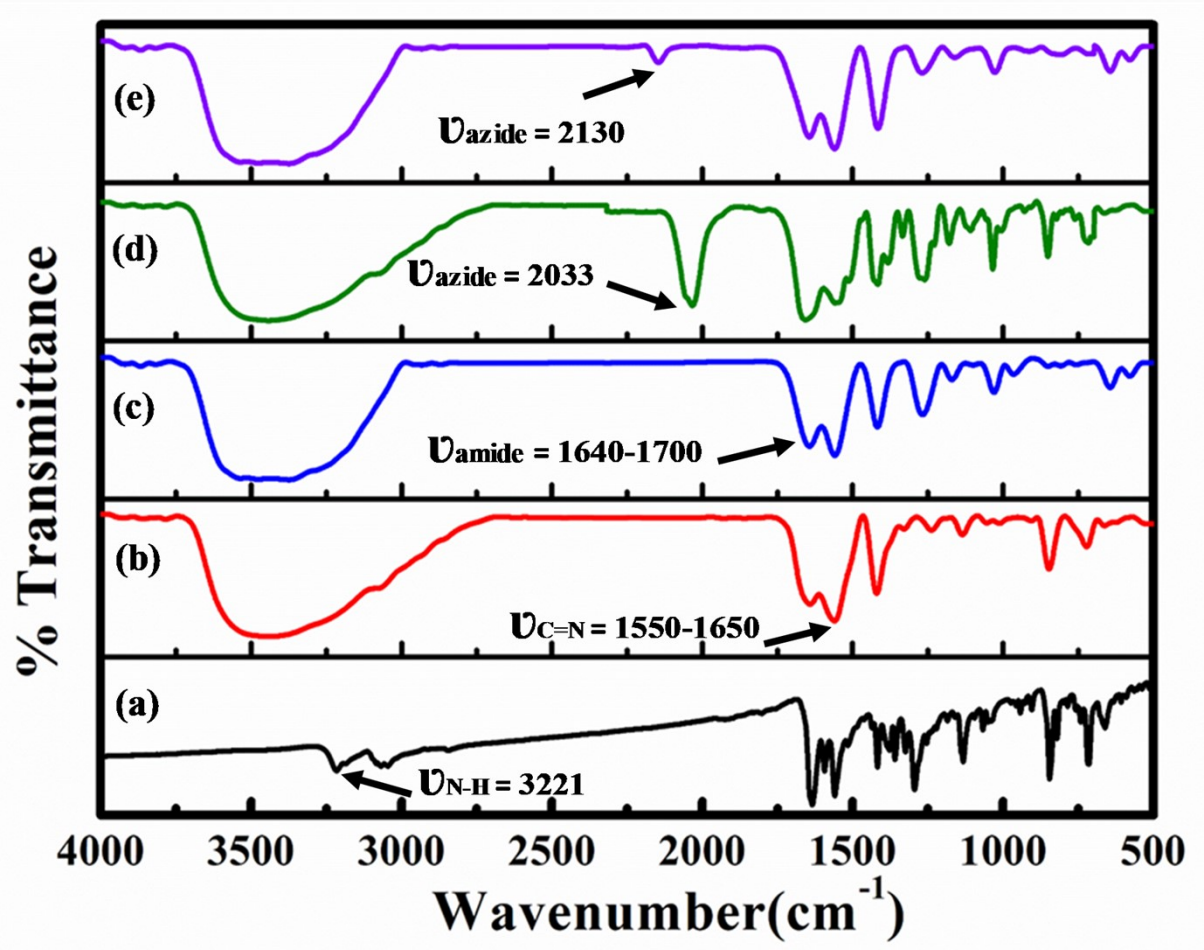

Fig. S5 FTIR stretching frequencies (in KBr pallet) of (a) **HL**, (b) complex **1**, (c) complex **2**, (d) complex **3** and (e) complex **4**, respectively.

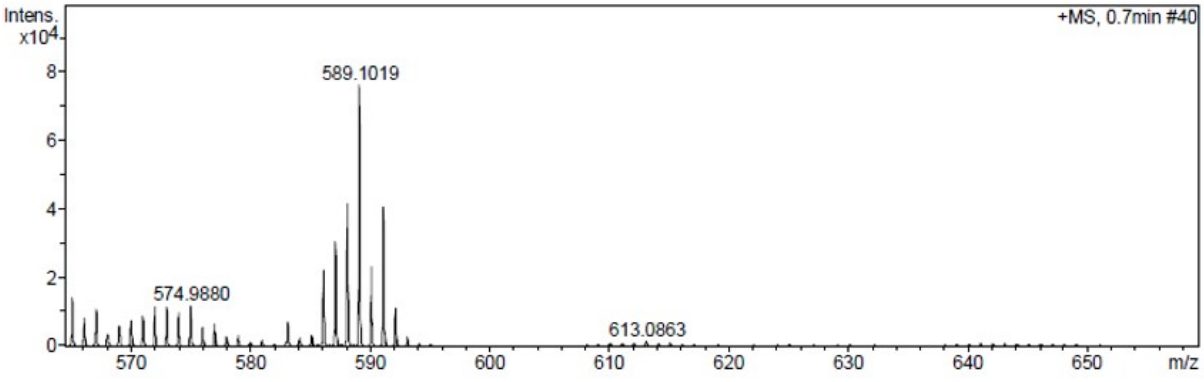

Fig. S6 ESI-MS of complex **1.**

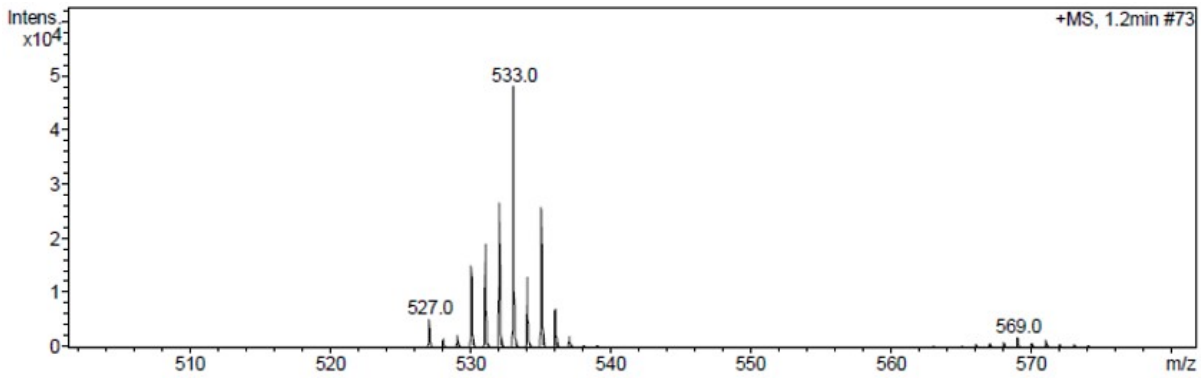

Fig. S7 ESI-MS of complex **2.**

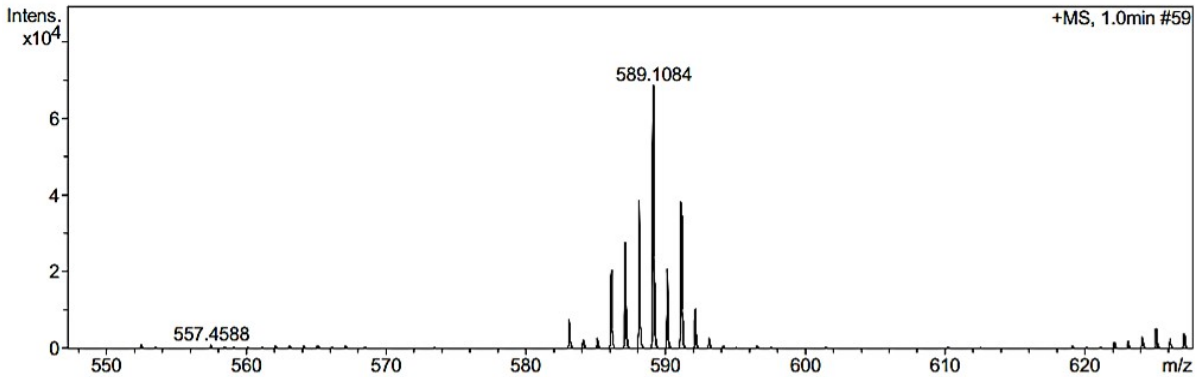

Fig. 8 ESI-MS of complex **3.**

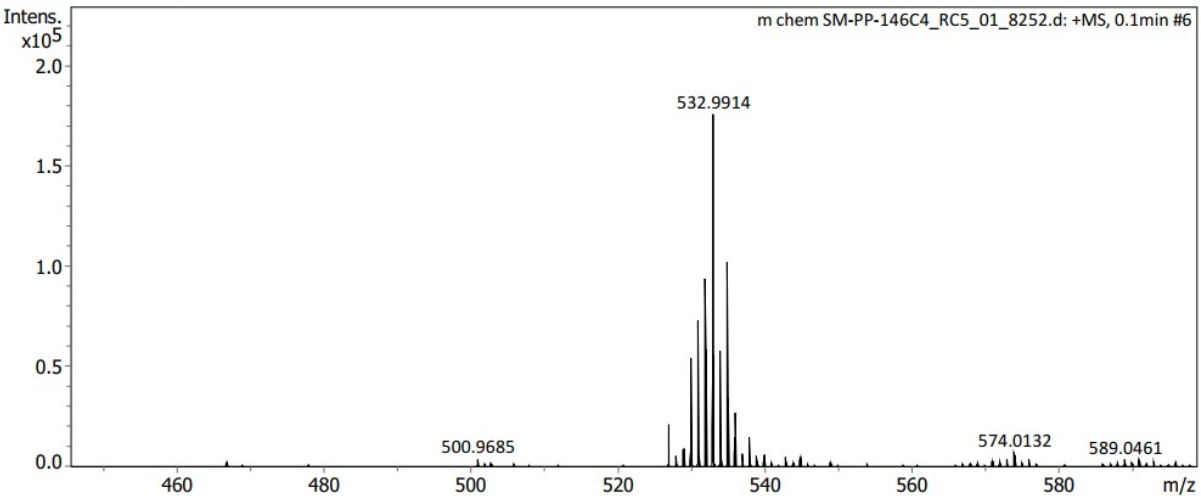

Fig. S9 ESI-MS of complex **4.**

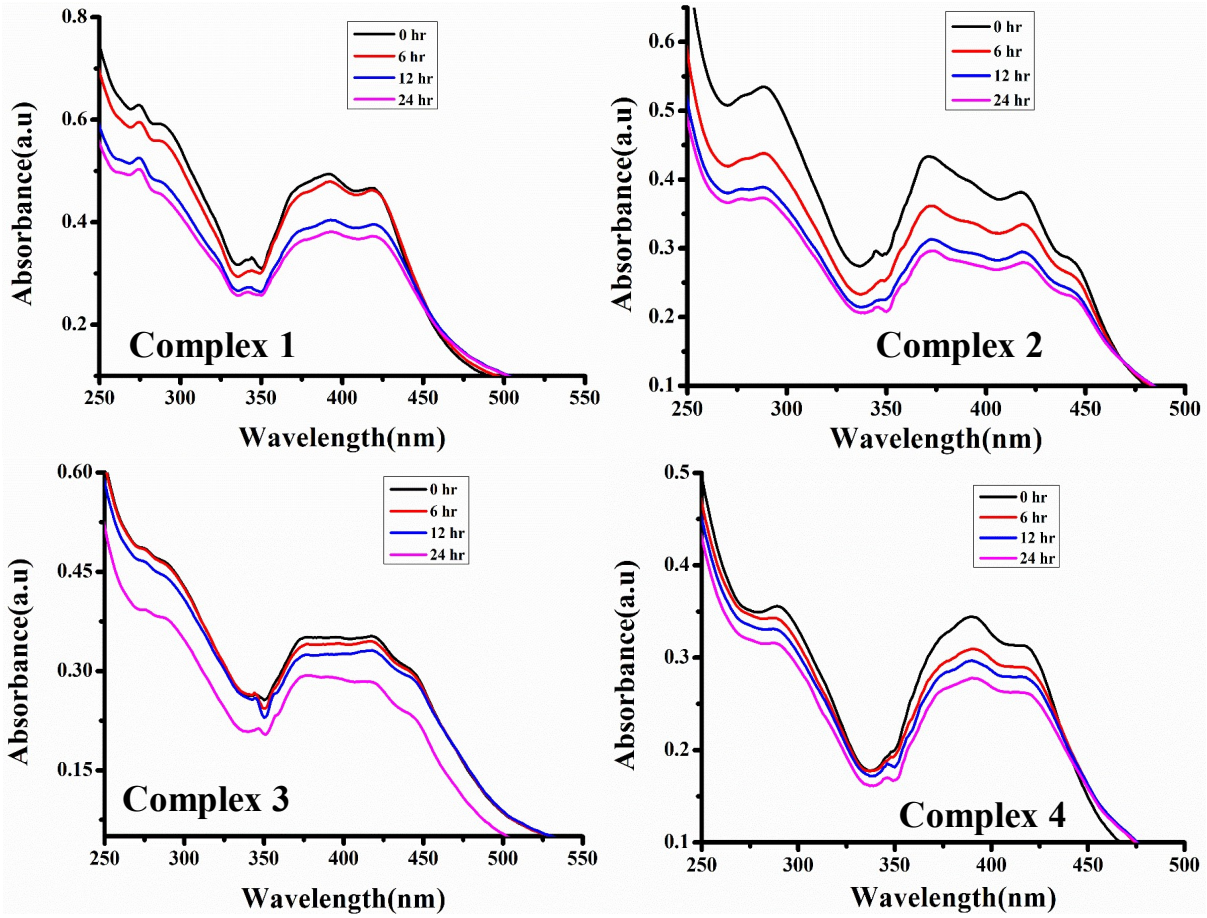

Fig. S10 Stability studies of the complexes 1-4 (1% DMSO in PBS Solution).

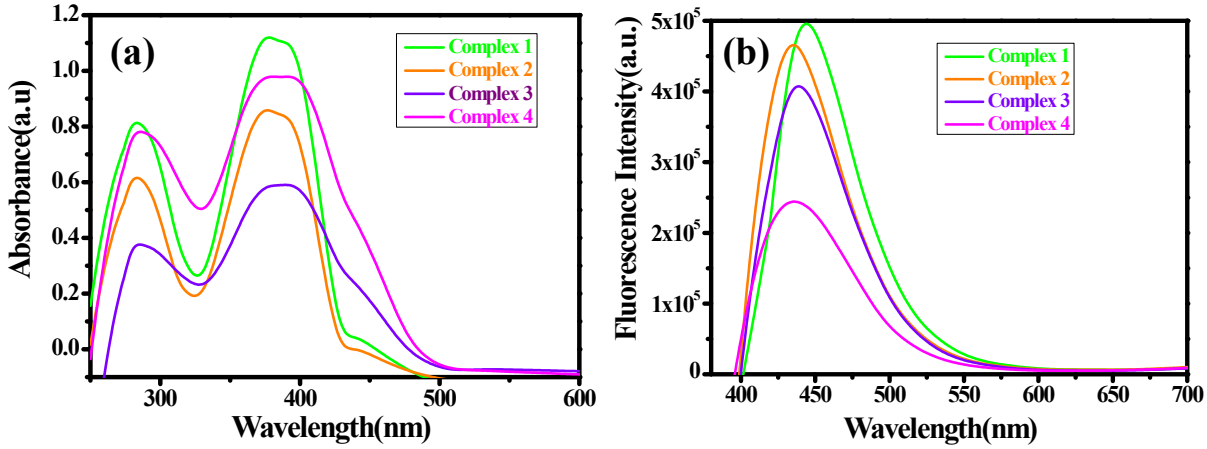

Fig. S11 (a) UV-Visible spectra (b) emission spectra of complexes **1-4** in DMSO.

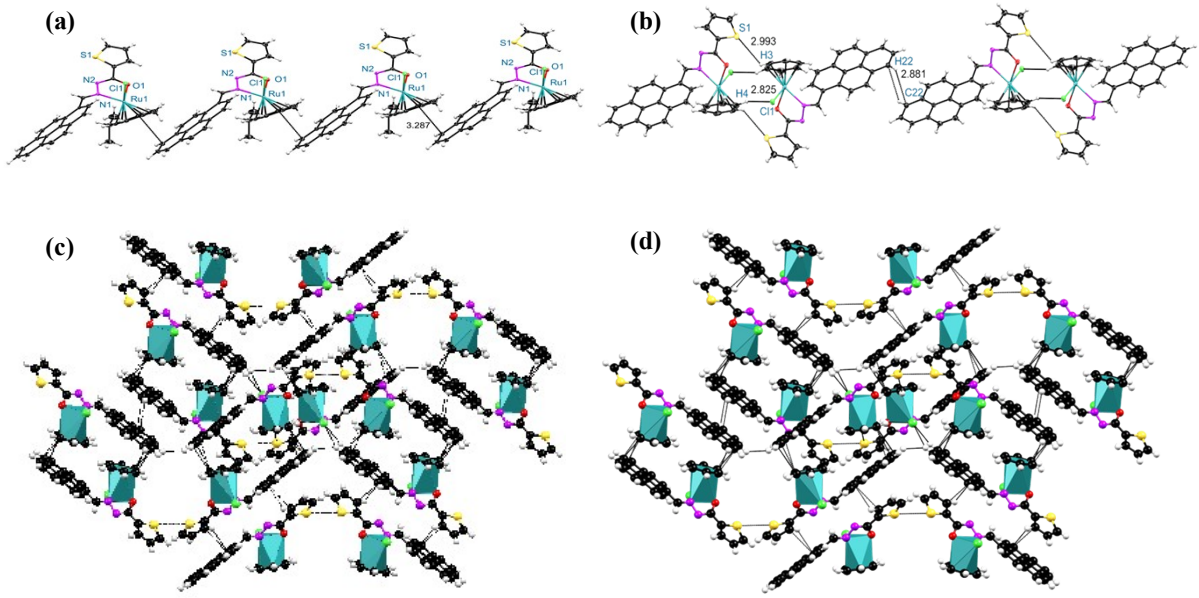

Fig. S12 Crystal polymeric framework. (a) and (b) 2D framework of complex **1** and complex **2.** (c) and (d) Supramolecular interaction in complex **1** and **2** *via* intermolecular hydrogen bonding and CH…π stacking interaction.

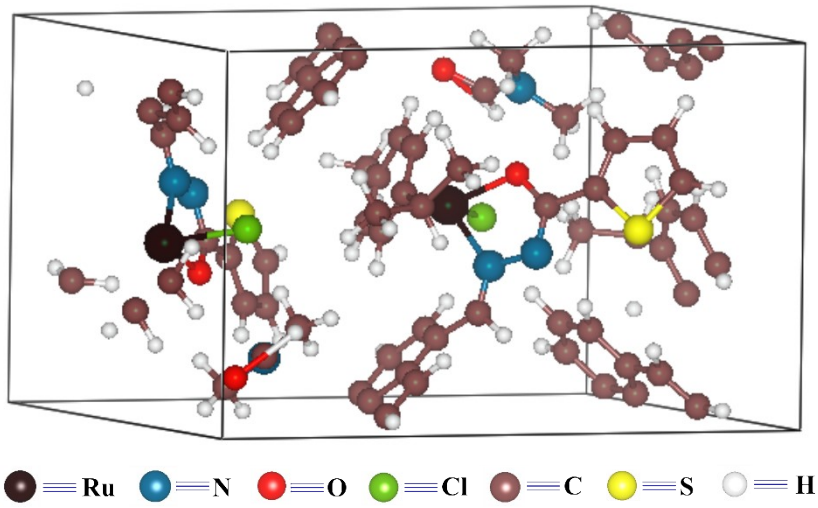

Fig. S13 The equilibrium 3D bulk crystal structure of the Complex **1** is depicted here, and the unit cell is highlighted by a cube.

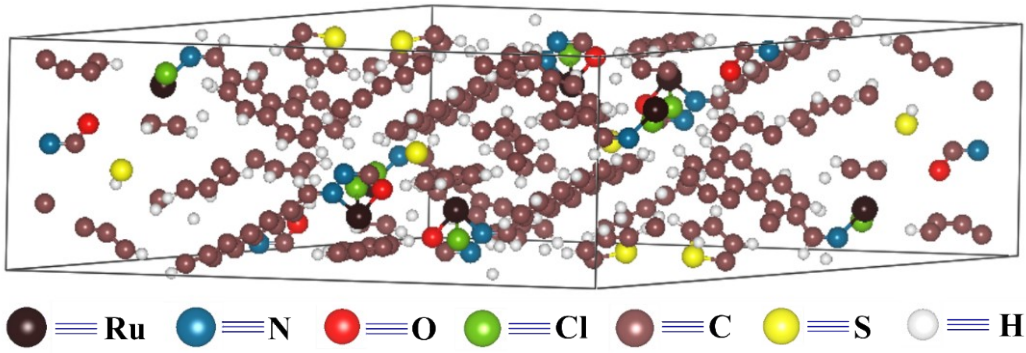

Fig. S14 The equilibrium 3D bulk crystal structure of the Complex **2** is depicted here, and the equilibrium unit-cell is shown by a cube.

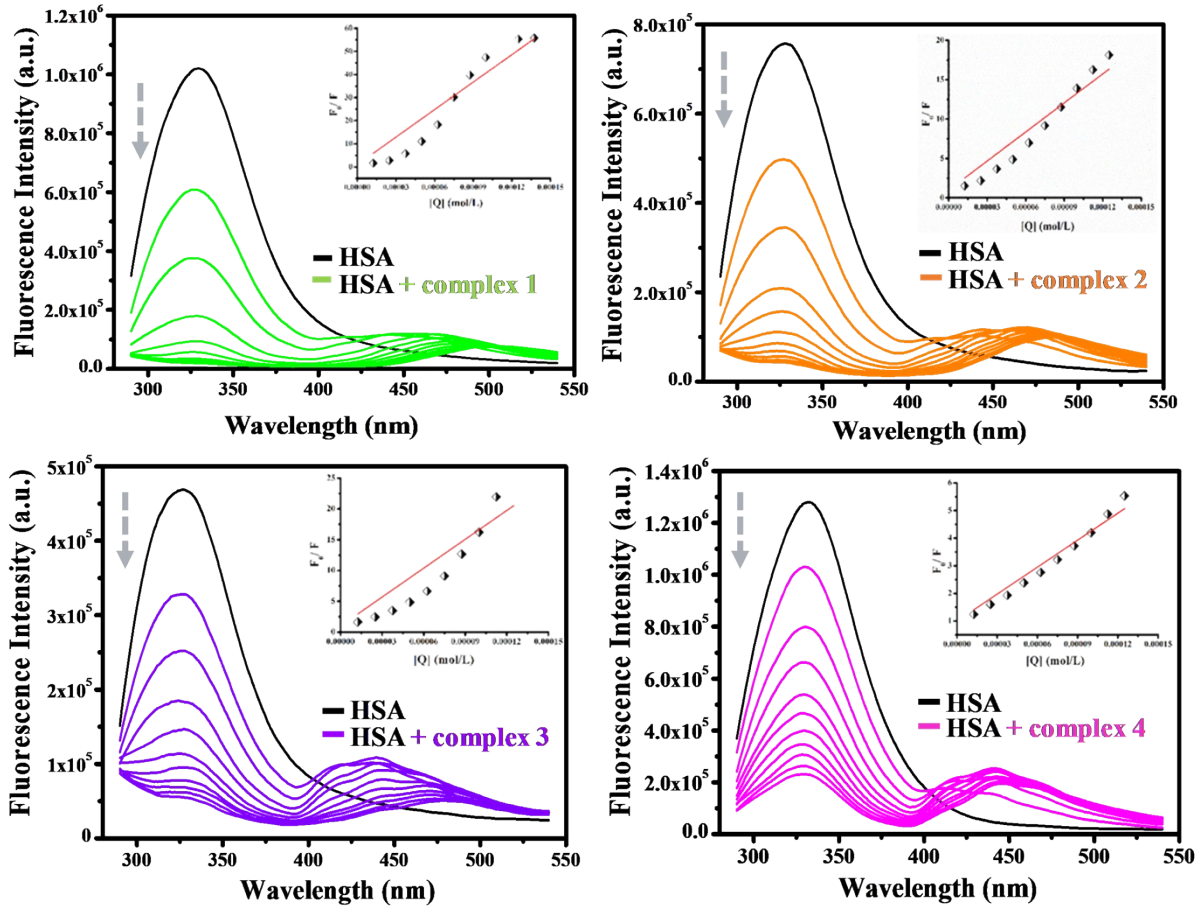

Fig. S15 Emission titration spectra of HSA (10 μM) in Tris-HCl buffer with complexes **1-4** (5-50 μM) at 298 K. Inset: Plots of F_0/F vs. [Q](mol/L) for HSA.

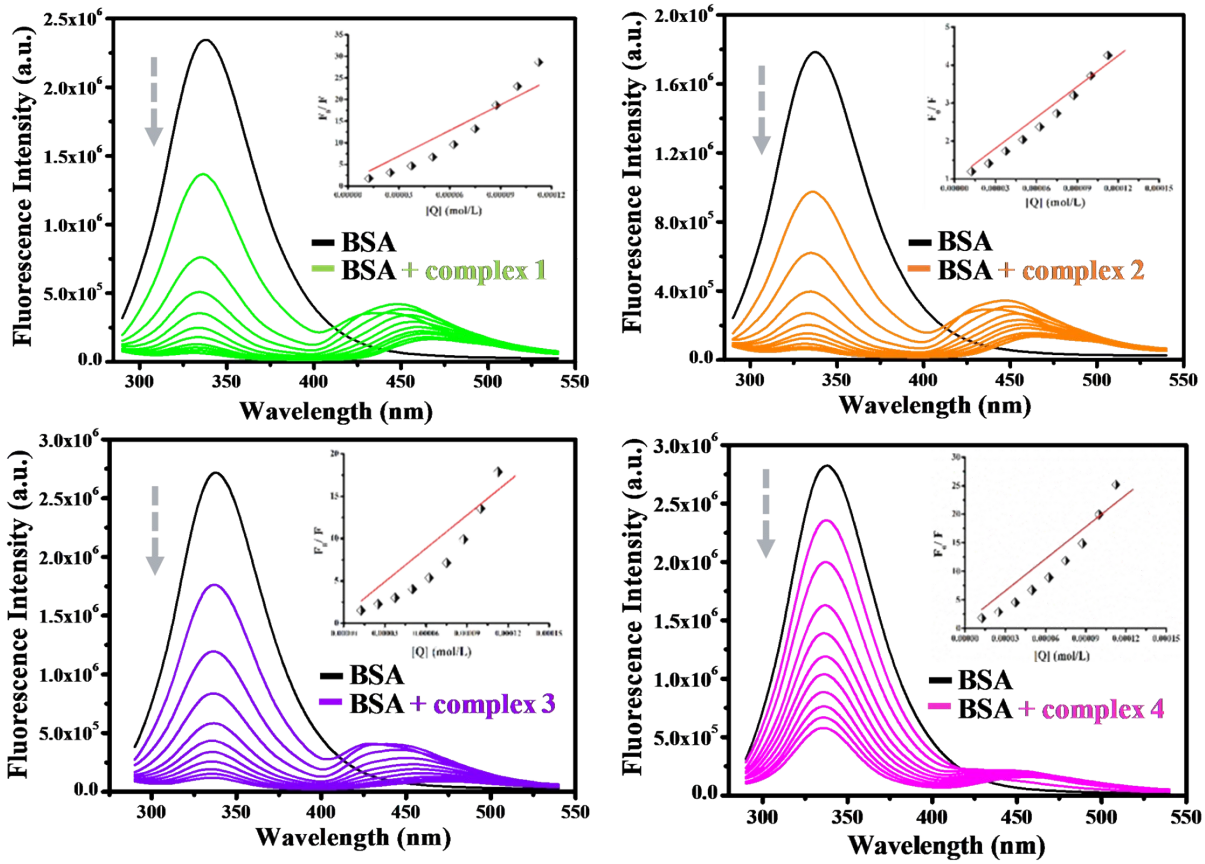

Fig. S16 Fluorescence quenching spectra of BSA (10 μM) at different concentrations (5-50 μM) of complexes **1-4** at 298 K.

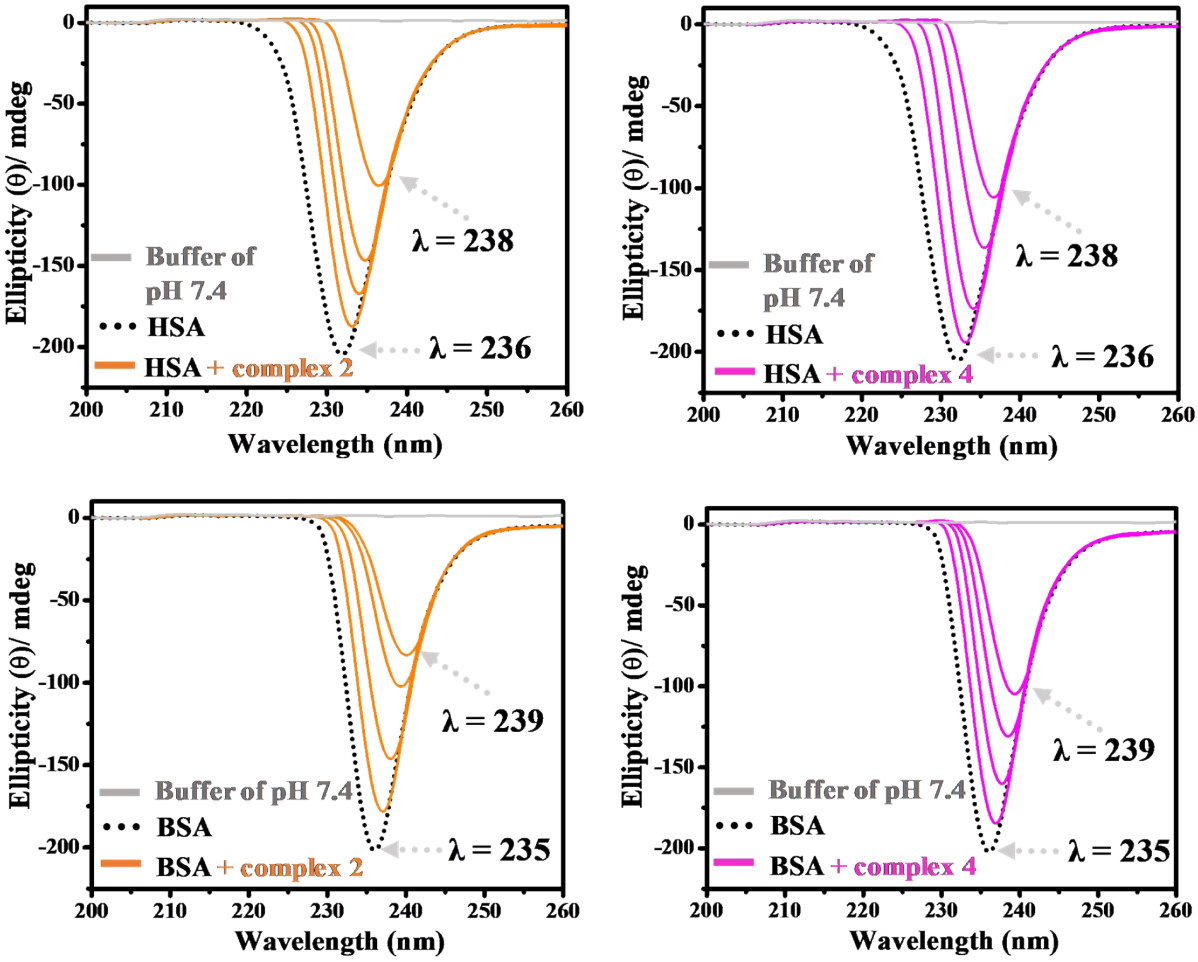

Fig. S17 BSA and HSA proteins (10 μM) Circular dichroism spectra with or without complex at different concentration (0-40 μM).

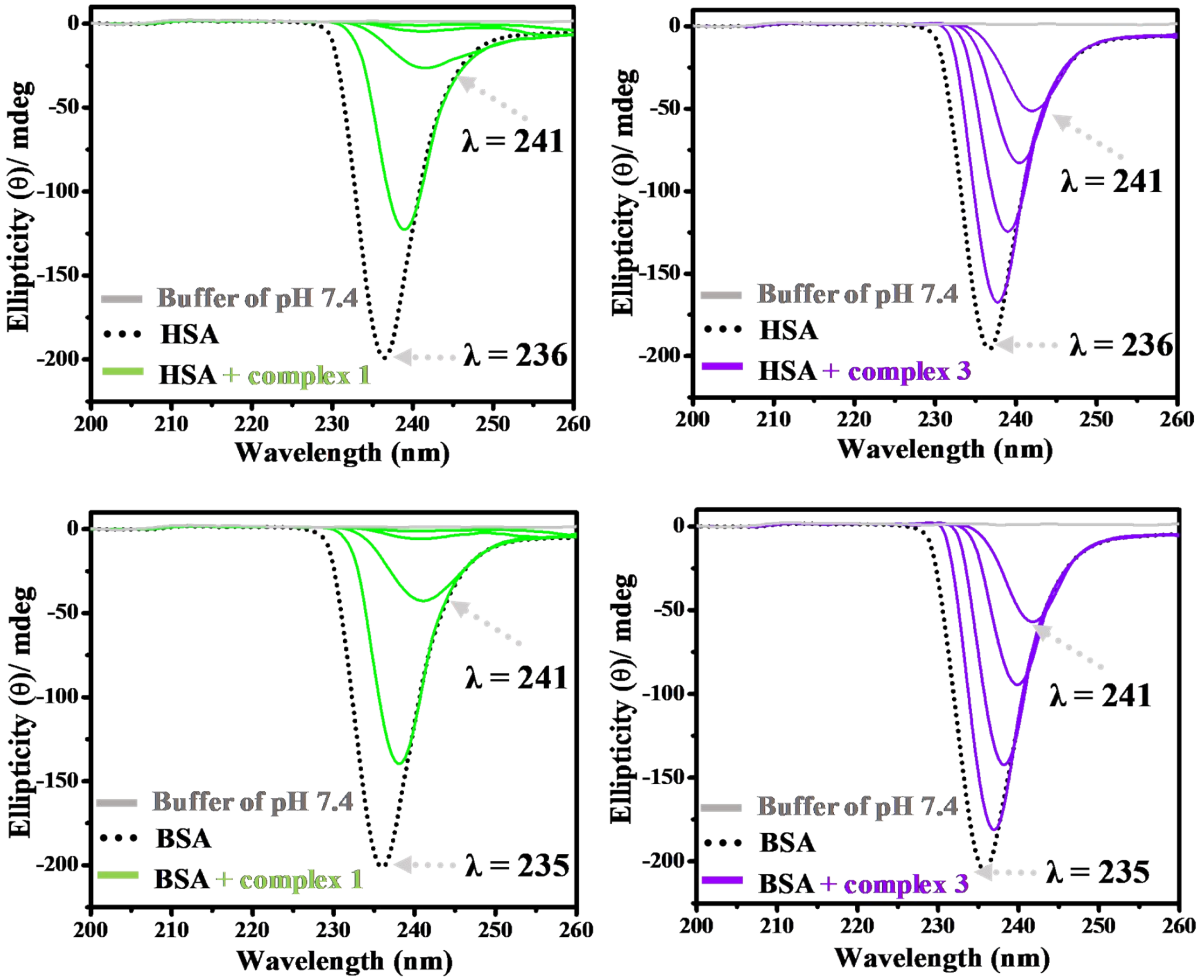

Fig. S18 BSA and HSA proteins (10 μM) Circular dichroism spectra with or without complex at different concentration (0-40 μM).

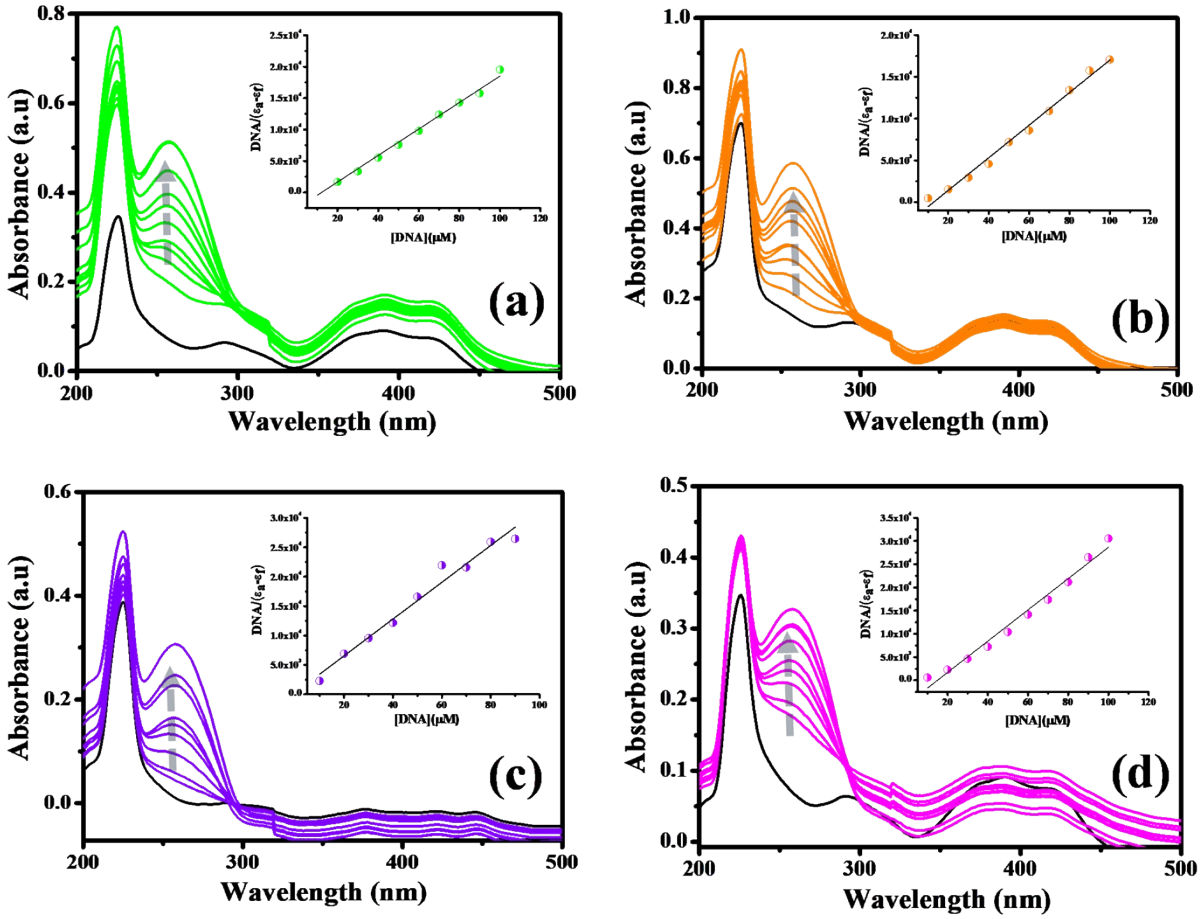

Fig. S19 Absorption titration spectra of complexes **1-4** with CT-DNA (a) complex 1 (b) complex 2 (c) complex 3 and (d) complex 4. Inset: Plots of [DNA] vs. [DNA]/εa − εf for the titration of CT-DNA with the complexes.

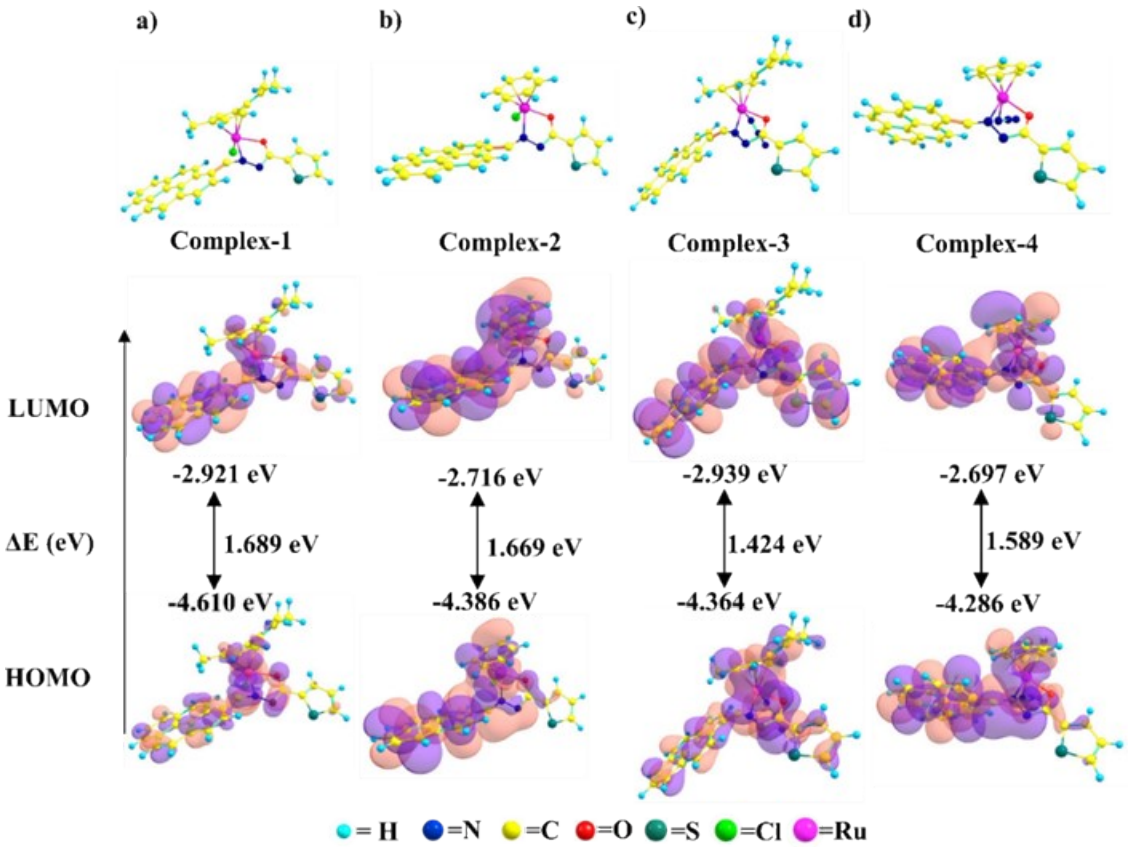

Fig. S20 The molecular orbitals analysis of the optimized complexes and their corresponding HOMO-LUMO energy gaps (a) complex 1 (b) complex 2 (c) complex 3, and (d) complex 4.

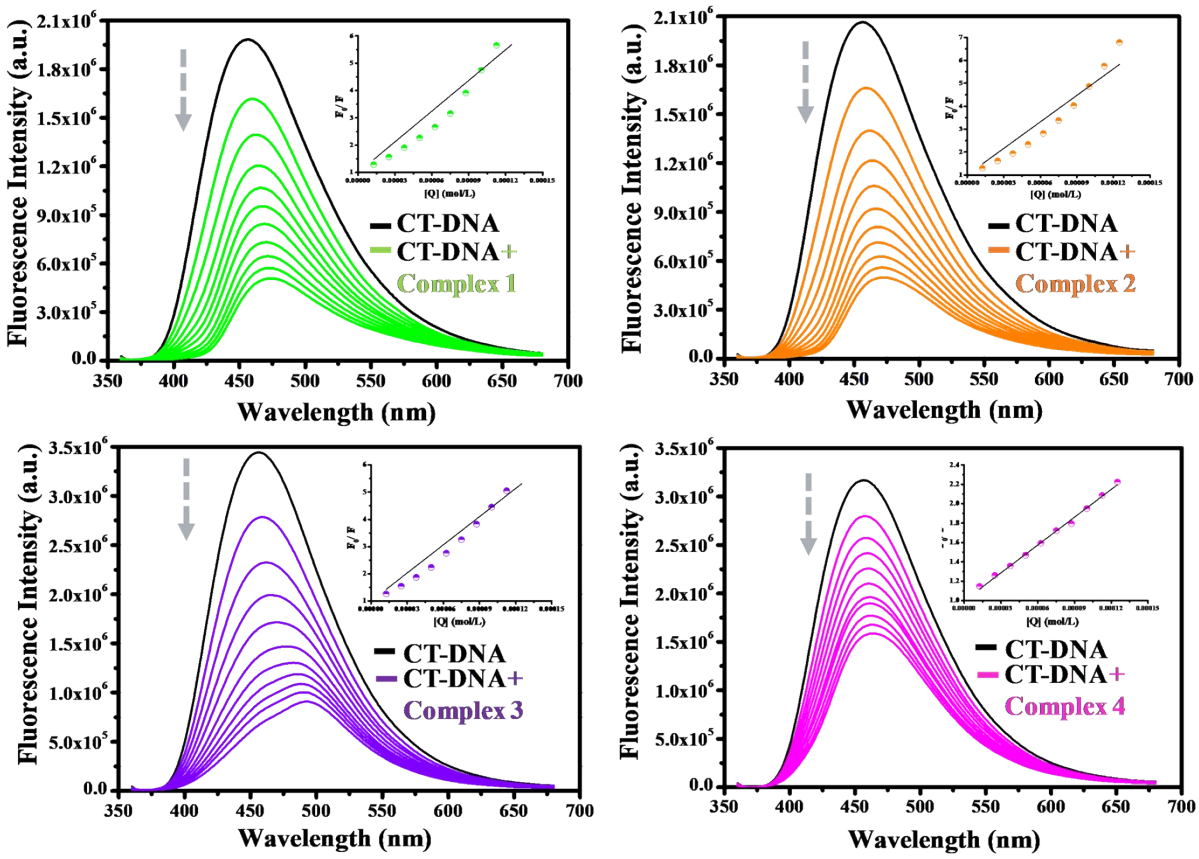

Fig. S21 Fluorescence quenching spectra of DAPI-DNA with complexes **1-4** (0-50 μM).

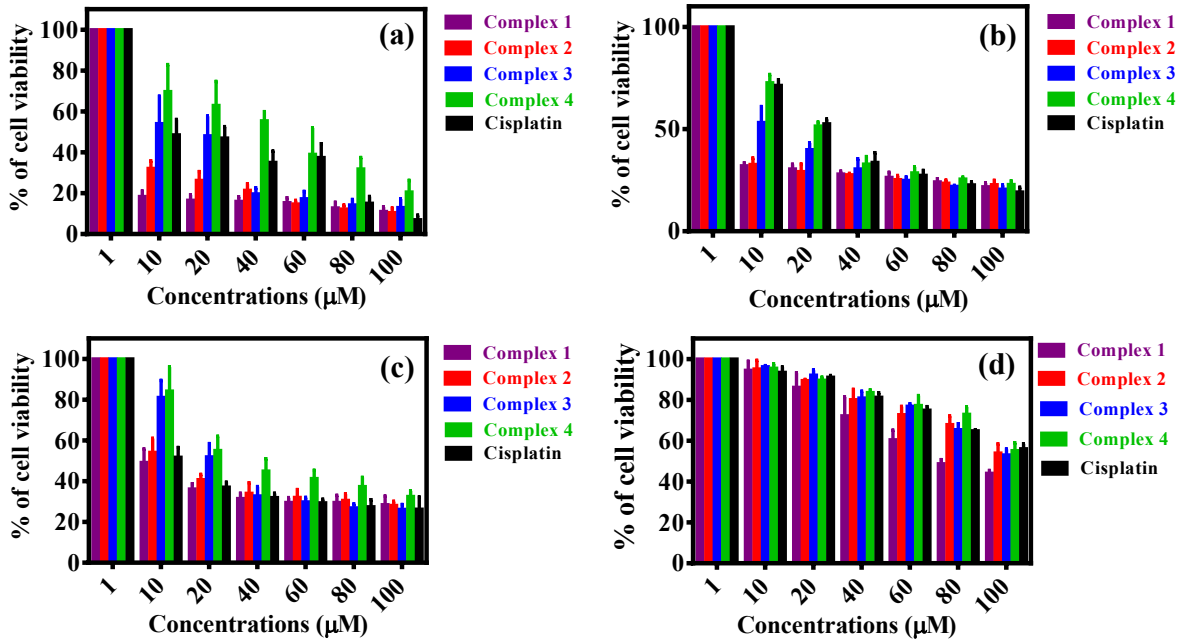

Fig. S22 % of cell viability of all synthesized complexes against respectively cancer cell lines (a) HeLa (b) A431 (c) MCF7 and (d) for HEK 293 (normal cell line).

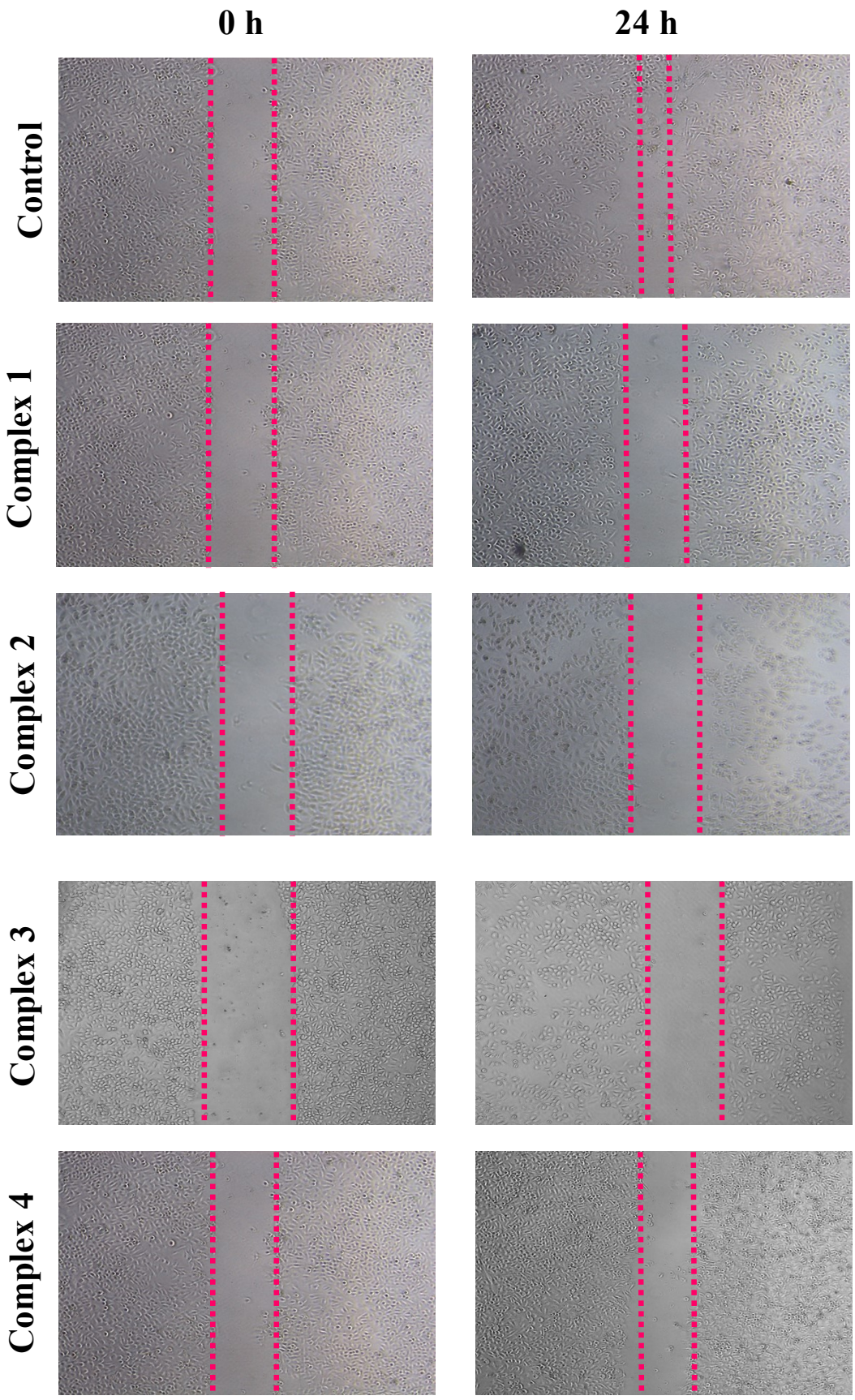

Fig. S23 Wound healing motility assay of HeLa untreated and treated cell with complexes **1-4**. Image were taken at 0 and 24 h.

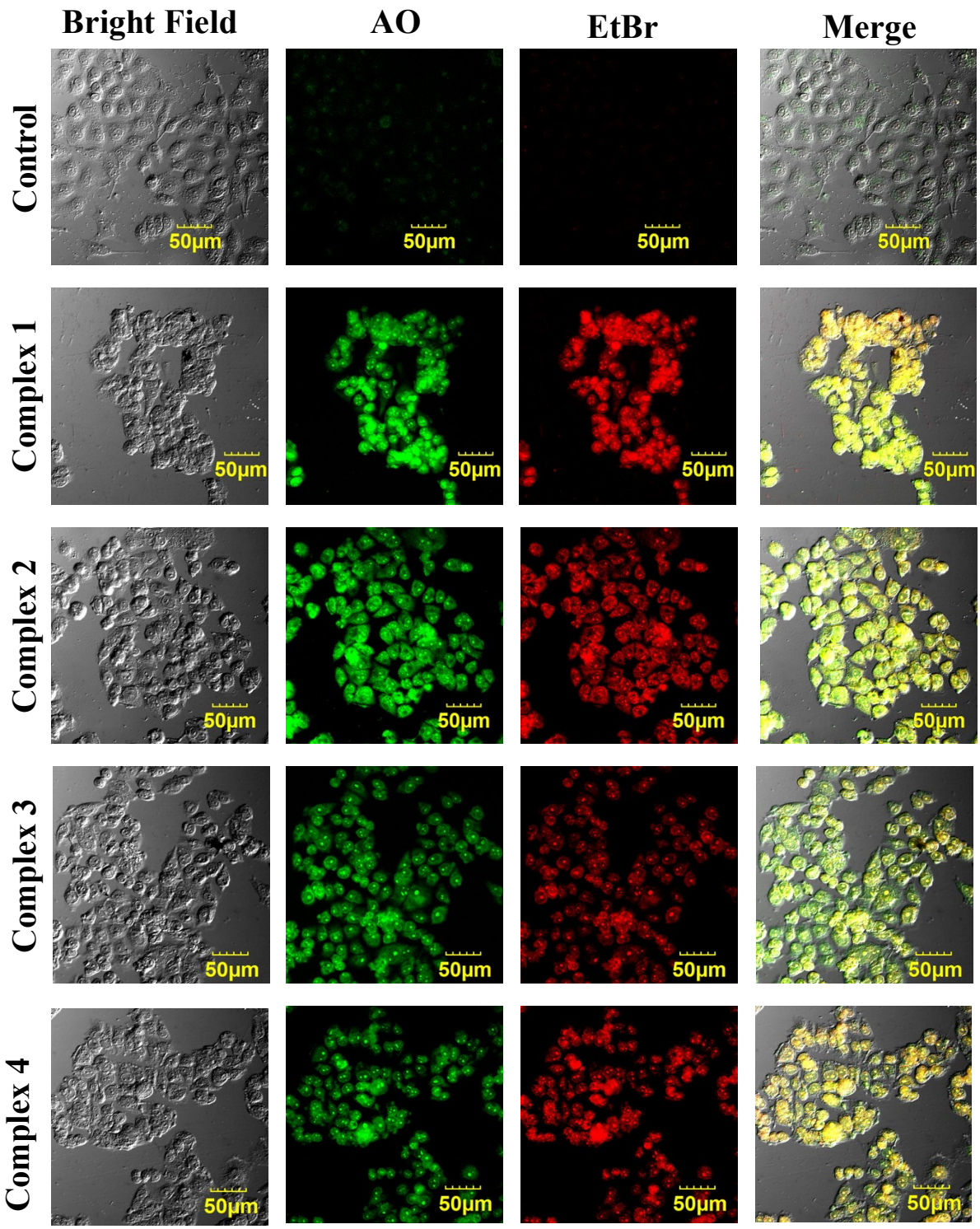

Fig. S24 Acridine orange and EtBr double staining confocal microscopy images of HeLa cells after complexes **1-4** treatment and cells without treatment as a control.

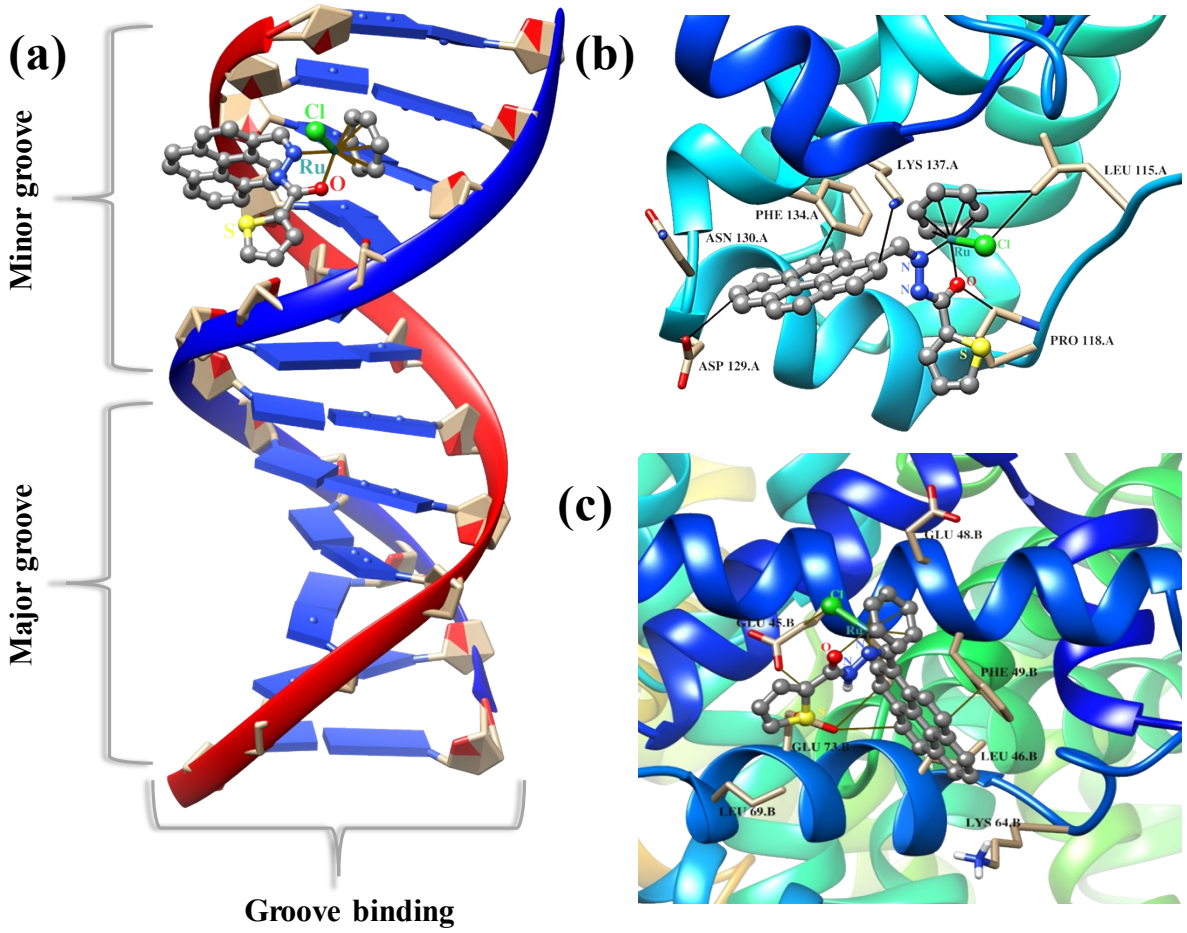

Fig. S25 Docking poses of complex **2** with (a) DNA (b) HSA and (c) BSA.

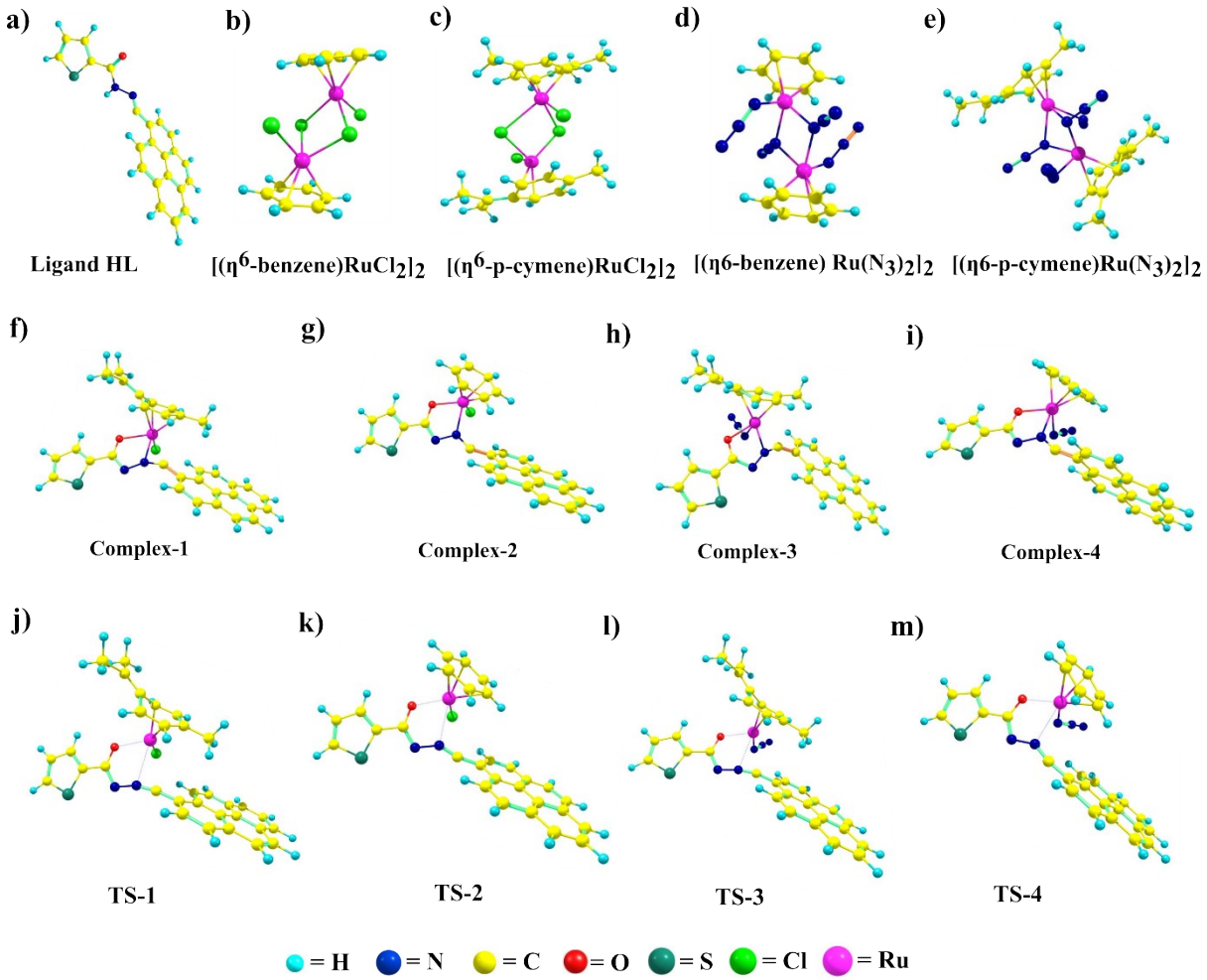

Fig. 26 Equilibrium geometries computed by the DFT method are presented here; a) Ligand, HL, b) [(η^6-benzene)$RuCl_2]_2$, c) [(η^6-p-cymene)$RuCl_2]_2$, d) [(η^6-benzene) $Ru(N_3)_2]_2$, e) [(η6-p-cymene)$Ru(N_3)_2]_2$, f) Complex **1**, g) Complex **2**, h) Complex **3**, i) Complex **4**, j) TS-1 is the transition state between A1 adduct and Complex **1** product. k) TS-2 is the transition state between A2 adduct and Complex **2** product. l) TS-3 is the transition state between A3 adduct and Complex **3** product. m) TS-4 is the transition state between A4 adduct and Complex **4** product.

Table S1 Selected bond lengths (Å) and bond angles (°) of complexes **1** and **2**.

Complex 1		**Complex 2**	
Ru1-Cl1	2.4025(11)	**Ru1-Cl1**	2.3985(6)
Ru1-O1	2.076(3)	**Ru1-O1**	2.0706(14)
Ru1-N1	2.090(3)	**Ru1-N1**	2.1044(15)
Ru1-C1	2.241(4)	**Ru1-C1**	2.177(2)
Ru1-C2	2.200(5)	**Ru1-C2**	2.188(2)

Ru1-C3	2.157(5)	**Ru1-C3**	2.180(2)
Ru1-C4	2.187(5)	**Ru1-C4**	2.186(2)
Ru1-C5	2.162(4)	**Ru1-C5**	2.167(2)
Ru1-C6	2.197(3)	**Ru1-C6**	2.188(2)
N1-N2	1.409(4)	**N1-N2**	1.408(2)
O1-C11	1.282(5)	**O1-C7**	1.290(2)
Cl1-Ru1-O1	85.01(9)	**Cl1-Ru1-O1**	85.80(4)
Cl1-Ru1-N1	86.45(9)	**Cl1-Ru1-N1**	86.22(4)
Cl1-Ru1-C1	90.51(9)	**Cl1-Ru1-C1**	126.50(7)
Cl1-Ru1-C2	109.71(13)	**Cl1-Ru1-C2**	96.33(6)
Cl1-Ru1-C3	145.67(11)	**Cl1-Ru1-C3**	89.40(7)
Cl1-Ru1-C4	167.15(13)	**Cl1-Ru1-C4**	110.37(7)
Cl1-Ru1-C5	129.33(10)	**Cl1-Ru1-C5**	146.95(8)
Cl1-Ru1-C6	98.74(9)	**Cl1-Ru1-C6**	163.72(6)
O1-Ru1-N1	76.66(13)	**O1-Ru1-N1**	76.54(5)
O1-Ru1-C1	129.25(14)	**O1-Ru1-C1**	147.10(8)
O1-Ru1-C2	98.65(16)	**O1-Ru1-C2**	162.70(8)
O1-Ru1-C3	88.75(15)	**O1-Ru1-C3**	125.27(8)
O1-Ru1-C4	107.83(15)	**O1-Ru1-C4**	95.25(8)
O1-Ru1-C5	144.30(12)	**O1-Ru1-C5**	88.61(7)
O1-Ru1-C6	165.80(15)	**O1-Ru1-C6**	110.42(7)
N1-Ru1-C1	153.57(14)	**N1-Ru1-C1**	97.40(7)
N1-Ru1-C2	162.92(15)	**N1-Ru1-C2**	120.68(8)
N1-Ru1-C3	124.78(13)	**N1-Ru1-C3**	157.39(8)
N1-Ru1-C4	96.84(15)	**N1-Ru1-C4**	161.15(9)
N1-Ru1-C5	94.04(14)	**N1-Ru1-C5**	123.97(8)
N1-Ru1-C6	117.11(15)	**N1-Ru1-C6**	98.69(7)

Table S2 Equilibrium structural parameters of the optimized crystal structure of the Complex 1 are summarized here.

Lattice parameters in Å	**Interfacial angles in degree (°)**	**Space group And Symmetry**	**Average bond distance between atoms (Å)**							
			N-N	**C-C**	**C-S**	**Ru-Cl**	**Ru-O**	**Ru-N**	**C-O**	**C-H**
a = 10.415, b = 16.831, c = 14.887	α = 90°, β =90° and γ = 90°	***P21*** Monoclinic	1.426	1.407	1.751	2.457	2.094	2.067	1.258	1.085

Table S3 Equilibrium structural parameters of the optimized crystal structure of the Complex **2** are reported here.

Lattice constants (a, b, c) in Å	**Interfacial angles (α, β, γ) in degree (°)**	**Space group And Symmetry**	**Various average equilibrium bond distances between atoms (Å)**							
			N-N	**C-C**	**C-S**	**Ru-Cl**	**Ru-O**	**Ru-N**	**C-O**	**C-H**
a = 24.049, b = 12.326, c = 30.732	α = 90°, β = 151.96° γ = 90°	***C2/c*** Monoclinic	1.425	1.408	1.753	2.443	2.080	2.088	1.301	1.081

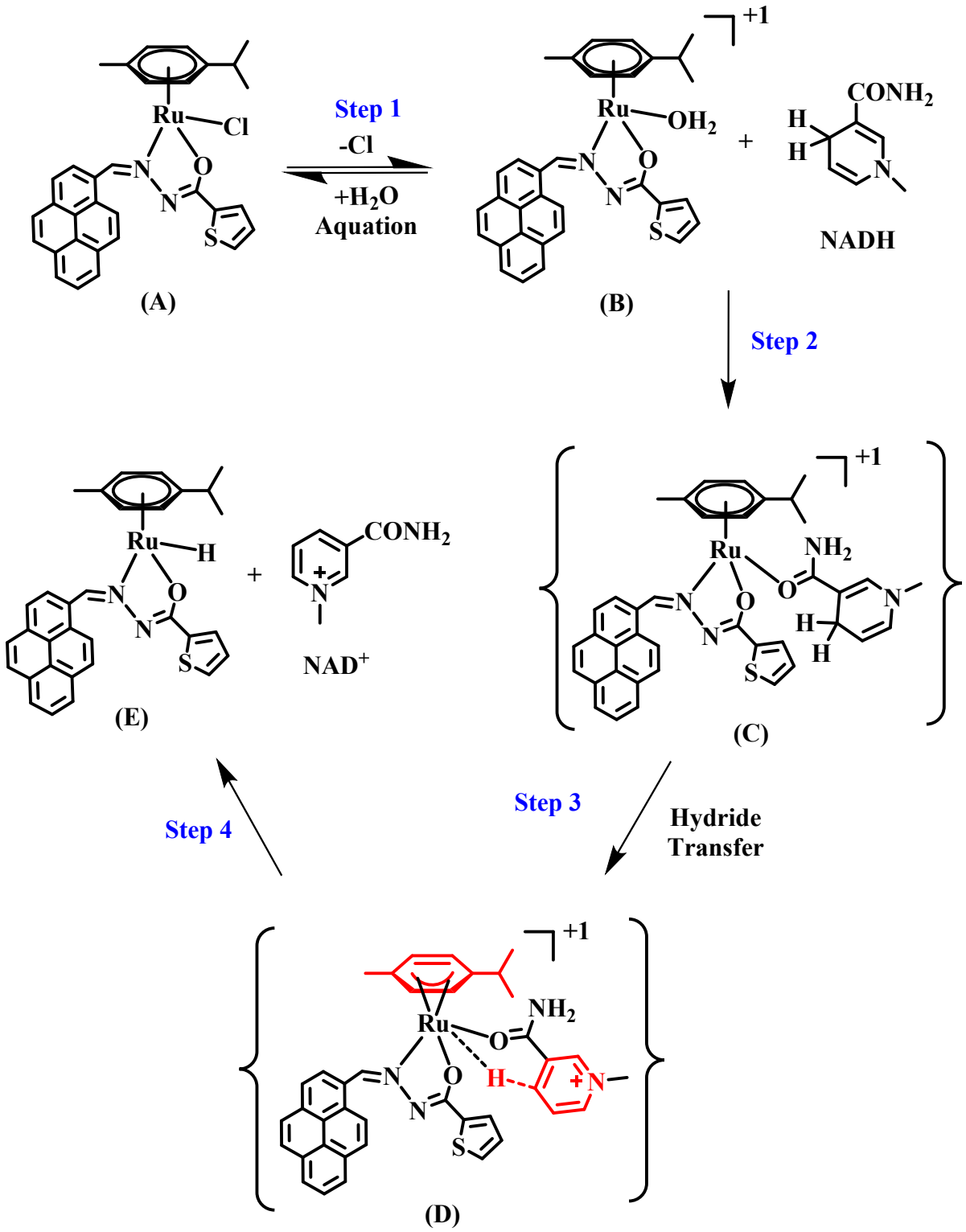

Scheme S1. The Probable mechanism of catalytic oxidation of NADH to NAD^+ for complex **1**.

References:

1 Bruker AXS, Madison, Wisconsin, USA., 6.01 edn., 1998, p. Data Reduction and Correction Program.

2 Bruker AXS., Madison, Wisconsin, USA., 2.01 edn., 1998, p. Bruker/Siemens Area Detector Absorption Correction Program.

3 SHELXTL-2014/7, Bruker AXS Inc., Madison, WI, USA, 2014.

4 B. Kumar Kundu, Pragti, S. M. Mobin and S. Mukhopadhyay, *Dalton Transactions*, 2020, **49**, 15481–15503.

5 Pragti, B. K. Kundu, C. Sonkar, R. Ganguly and S. Mukhopadhyay, *Polyhedron*, 2021, **207**, 115379.

6 M. Das, B. K. Kundu, R. Tiwari, P. Mandal, D. Nayak, R. Ganguly and S. Mukhopadhyay, *Inorganica Chimica Acta*, 2018, **469**, 111–122.

7 X. Liu, H. Hao, X. Ge, X. He, Y. Liu, Y. Wang, H. Wang, M. Shao, Z. Jing and L. Tian, *Journal of inorganic biochemistry*, 2019, **199**, 110757.

8 C. Sonkar, N. Malviya, R. Ranjan, S. Pakhira and S. Mukhopadhyay, *ACS Applied Bio Materials*, 2020, **3**, 4600–4612.